JOURNAL OF SOLID STATE CHEMISTRY 105, 480–488 (1993)

Tunnel Cation Ordering in K- and Rb-Octatitanates

TAKAYOSHI SASAKI,* MAMORU WATANABE, YOSHINORI FUJIKI, AND YOSHIZO KITAMI

National Institute for Research in Inorganic Materials, 1-1 Namiki, Tsukuba, Ibaraki 305, Japan

Received July 9, 1992; in revised form November 30, 1992; accepted December 2, 1992

The electron diffraction patterns for the rubidium octatitanate $Rb_2Ti_8O_{17}$ exhibited commensurate superlattice reflections attributable to doubled dimensions of the *a*, *b*, and *c* axes. The three-dimensional superstructure was unstable under an intense beam irradiation where a correlation parallel to the *a* axis was destroyed. This is in line with the powder X-ray diffraction data where the superlattice reflections disappeared around 600°C. The reconstruction of the reciprocal lattice from the electron diffraction data suggests a twinning of supercells connected with (010) plane. The structural models are developed in terms of Rb ion ordering. Two configurations of unit tunnel contents, [Rb–□–Rb–□] and [□–Rb–□–Rb] (□, vacancy; [ ], unit tunnel limits along the *c*) arrange alternately along the *b* and *c* axes, resulting in a two-dimensional sheet, which is then stacked along the *a* axis. The twin formation as well as the three-dimensional/two-dimensional transition is well explained on the basis of the structural models. The K ion distribution in $K_2Ti_8O_{17}$ is also discussed in relation to the Rb ion ordering.

Introduction

The octatitanate $M_2Ti_8O_{17}$ (M = K, Rb) (*1–3*), one of the alkali poorest members among the classes of titanates of composition $A_2O \cdot nTiO_2$ (A, alkali metal) (*4–11*), is characterized by an open host framework. The low alkali content gives rise to inadequate local charge neutrality, which makes the compound metastable according to Pauling's electrostatic valence rule (*12*). The structure would be stabilized by incorporating one additional cation per formula unit. One of such compositions is the mixed valent $K_3Ti_8O_{17}$, which has been synthesized by the electrolysis of molten system K_2O–TiO_2–Nb_2O_5 (*13*) and by the reductive K insertion on $K_2Ti_8O_{17}$ (*3*).

A metastable open structure like the above may exhibit some distinctive properties, e.g., ionic conduction, host–guest interaction. It is, therefore, of great interest to study a cation distribution in open host frameworks. We have carried out the structural characterizations for $K_2Ti_8O_{17}$ and $Rb_2Ti_8O_{17}$ paying particular attention to the accommodation ways of the tunnel cations (*14*). Figure 1 illustrates the polyhedral representation of the structure. The linkage of TiO_6 octahedra in the framework produces the one-dimensional tunnel, parallel to the *b* axis, a cross section of which is enclosed by one and four octahedra thickness. Alkali metal ions are accommodated in two kinds of distorted cubic positions in the tunnel (M_1 and M_2 in Fig. 1). Only two of four sites in a unit tunnel (M_1, M_1', M_2, M_2') are occupied, leaving two others vacant. The Rietveld refinement revealed that K ions are statistically distributed between M_1 and M_2 sites (*14*). The ionic conduction reported (*15*) may be attributed to a hopping migration of K ions between these two sites. In contrast, a superstructure has been discerned for

*To whom correspondence should be addressed.

0022-4596/93 $5.00

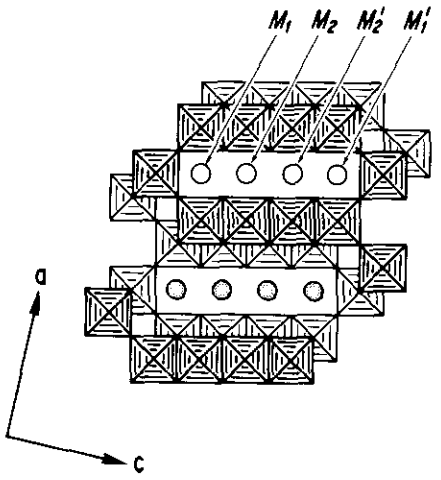

FIG. 1. Ideal representation of the crystal structure for octatitanate $M_2Ti_8O_{17}$ (M = K, Rb) viewed down along the b axis. The compound crystallizes in the monoclinic system, space group $C2/m$ with cell parameters a = 15.678(2), b = 3.775(1), c = 11.951(1) Å, and β = 95.67(1)° for $K_2Ti_8O_{17}$, and a = 15.961(3), b = 3.786(1), c = 11.918(2) Å, and β = 96.05(2)° for $Rb_2Ti_8O_{17}$, respectively (*3*). Two of four pseudocubic sites (designated as the circles; M_1, M_1', M_2, M_2') in a unit tunnel are occupied by the cations. Symmetry relationship. M_1, x, y, z; M_1', $1 - x$, y, $1 - z$; similar for M_2 and M_2'. The heavily marked octahedra and stippled circles are on the plane of y = 0.

$Rb_2Ti_8O_{17}$ suggesting an ordered configuration of Rb ions (*14*). This paper follows up the preceding study (*14*) and describes the analysis on the superstructure for $Rb_2Ti_8O_{17}$ studied by electron diffraction and X-ray powder diffraction techniques. The structural models are developed for $Rb_2Ti_8O_{17}$ on the basis of the reconstructed reciprocal lattice. Furthermore, they are extended to discuss the accommodation manner of K ions in $K_2Ti_8O_{17}$.

Experimental

Fibrous octatitanate crystals (~30 μm in thickness and ~500 μm in length) have been prepared according to the process described previously (*3*).

Electron diffraction data were collected by a JEOL JEM-2000EX electron microscope operated at 200 kV with a double-tilting goniometer (±25°). Crystal fragments, sliced by a LBK Microtome, were supported on a holey carbon copper grid.

The powder X-ray diffraction patterns were recorded using a Rigaku Denki RAD-2B diffractometer equipped with graphite-monochromatized Cu$K\alpha$ radiation (λ = 1.5405 Å).

Results and Discussion

Reconstruction of Superlattice by the Electron Diffraction Technique

The reciprocal lattices for $K_2Ti_8O_{17}$ and $Rb_2Ti_8O_{17}$ were explored by recording a series of electron diffraction patterns evolved by tilting a crystal fragment around the a^* and c^* axes. It was confirmed that the latter gave superlattice reflections besides the diffraction spots from the ordinary cell while the former did not. Thus, hereunder, we will concentrate on the case for ordered $Rb_2Ti_8O_{17}$.

The rotation around the a^* recognized six kinds of the reciprocal lattice sections, $h0l^*$, $hk5k^*$, $hk4k^*$, $hk3k^*$, $hk2k^*$, hkk^*. The former four are shown in Fig. 2 and the others are deposited. The superlattice spots were observed in the reciprocal lattice sections of $hk5k^*$, $hk3k^*$, and hkk^* but not in $h0l^*$, $hk4k^*$, and $hk2k^*$. The superlattice reflections can be indexed in terms of odd half integral multiples of all three axes, a^*, b^*, and c^*, being three dimensionally commensurate with the sublattice.

With respect to the tilt around the c^* axis, six diffraction patterns were also examined. The diffraction patterns of kkl^*, $3kkl^*$, and $5kkl^*$ exhibited the superlattice satellites with indices (h/2, k/2, l/2) where h, k, and l are odd. This agrees with the superlattice uncovered by the rotation around the a^*.

It was puzzling at a first glance because the zones such as $hk0^*$, $2kkl^*$, and $4kkl^*$ sometimes appeared to have superlattice reflections positioned at (h, k/2, l/2) where k is odd/even for odd/even l, e.g., (0, $\frac{1}{2}$, $\frac{1}{2}$),

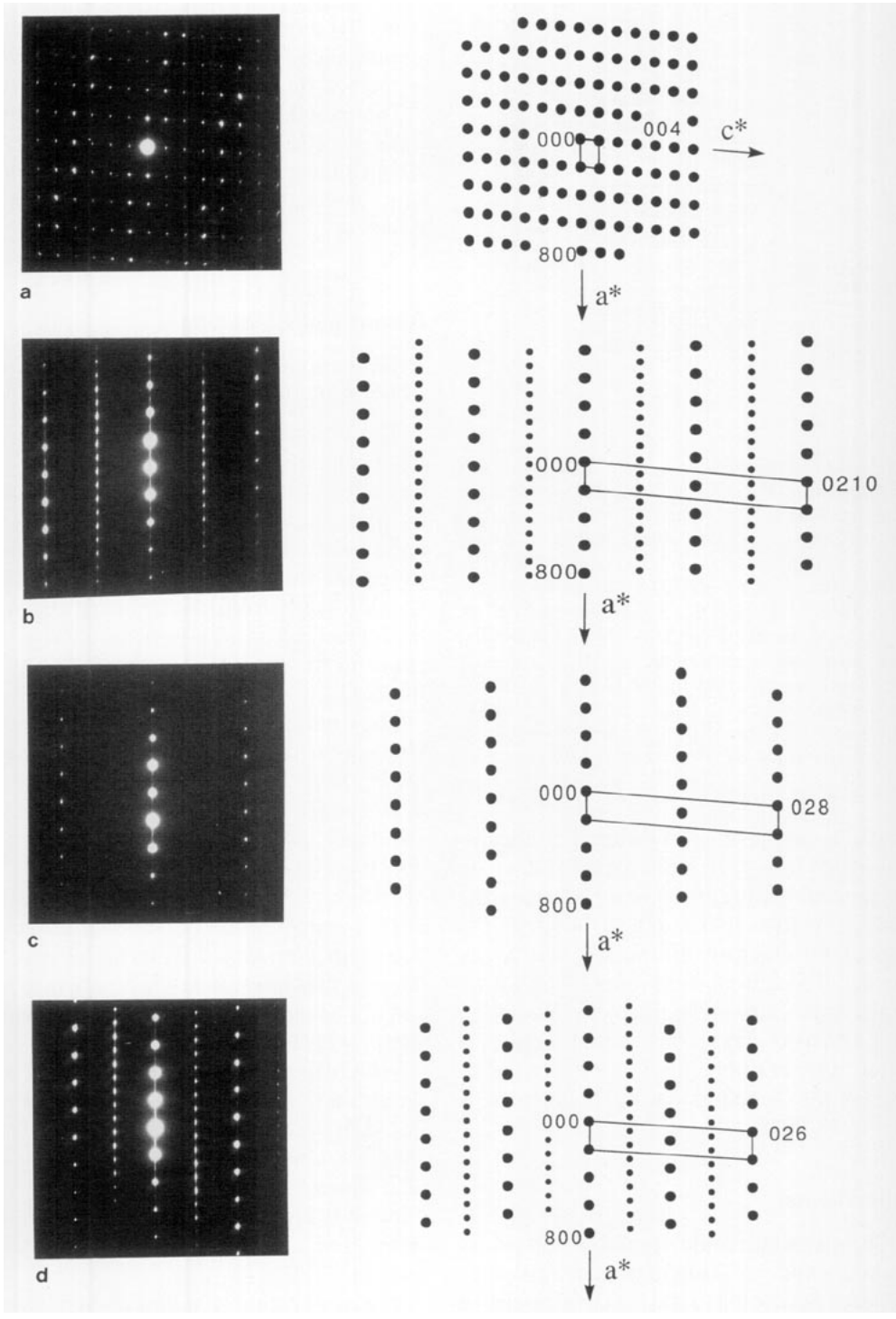

FIG. 2. Electron diffraction patterns for $Rb_2Ti_8O_{17}$ taken by rotation around the a^*. (a) $h0l^*$, (b) $hk5k^*$, (c) $hk4k^*$, and (d) $hk3k^*$. The large and small dots correspond to the sub- and superlattice reflections, respectively. The subcell is enclosed by solid lines.

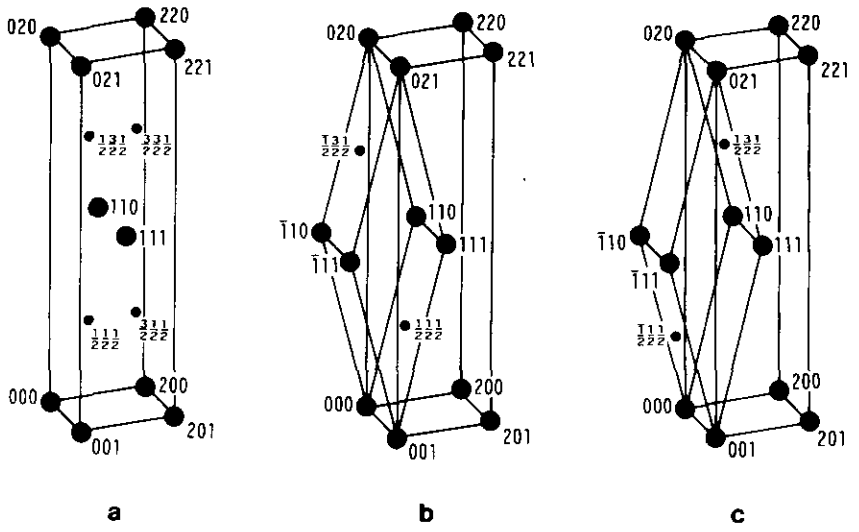

FIG. 3. (a) Reconstructed reciprocal lattice for $Rb_2Ti_8O_{17}$. (b), (c) Twin components of the reciprocal superlattice. Larger dot, subcell spots; smaller dot, supercell spots.

$(1, \frac{1}{2}, \frac{1}{2})$, (010), (210). This is in contradiction to the data deduced from the a^* axis tilt. Their intensities were variable from specimen to specimen. An elaborate cross check on the diffraction patterns evolved by the rotation around the a^* and c^* led to a conclusion that these spots were not genuine Bragg reflections but cross sections of diffuse tails, extending along the a^*, from Bragg spots off the zone plane. The lengths of the diffuse tails varied, as detailed in the next section, depending on individual crystallites and beam irradiation. This made the intensities of the spurious superspots changeable.

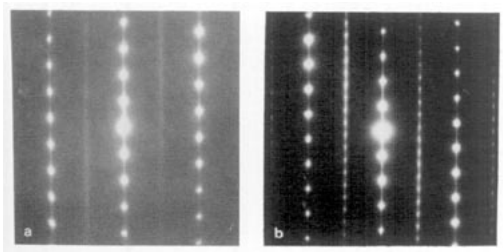

FIG. 4. Reciprocal zone of $hk3k^*$ showing various degree of disorder along the a^*. (a) continuous rod, (b) intermediate. Compare these with the pattern in Fig. 2d exhibiting the sharp superlattice spots.

Figure 3a shows the reciprocal lattice for $Rb_2Ti_8O_{17}$ which was rebuilt from the electron diffraction data above: The C-base centered subcell contains four supercell satellites $[(\frac{1}{2}, \frac{1}{2}, \frac{1}{2}), (\frac{3}{2}, \frac{1}{2}, \frac{1}{2}), (\frac{1}{2}, \frac{3}{2}, \frac{1}{2}), (\frac{3}{2}, \frac{3}{2}, \frac{1}{2})]$. The real supercell has doubled dimensions for all three crystallographic directions with respect to the subcell.

The observed reciprocal lattice could not be assigned to any 1 of 14 Bravais lattices. We assume that the lattice is described as a twin combination of the B-base centered triclinic cells, shown in Figs. 3b and 3c, the individuals of which are twinned with (010). The supercells are related to the subcell by the following equations.

$$\mathbf{a}_s^* = (\pm\mathbf{a}_0^* + \mathbf{b}_0^*)/2$$
$$\mathbf{b}_s^* = (\mp\mathbf{a}_0^* + \mathbf{b}_0^*)/2$$
$$\mathbf{c}_s^* = \pm\mathbf{c}_0^*,$$

where subscript "0" and "s" denotes sub- and supercell, respectively.

We attempted to confirm the twinning by the dark field imaging technique. However, this was unsuccessful since neighboring superlattice spots from the twin individuals, e.g., $(\frac{1}{2}, \frac{1}{2}, \frac{1}{2})$ and $(\bar{\frac{1}{2}}, \frac{1}{2}, \frac{1}{2})$, could not be sepa-

rated even by use of the smallest apertures available.

Three-Dimensional/Two-Dimensional Transition

The lateral spreading of the superlattice spots along the a^* is indicative of a short range of coherence in that direction. The rows of the spots along the a^* sometimes became continuous under intense beam irradiation, as exemplified in Fig. 4. The doubled periodicities with respect to the b^* and c^* were preserved after the correlation along the a^* was lost. This gives an explanation for the spurious supercell spots observed in the zones of $hk0^*$, $2kkl^*$ and $4kkl^*$.

The degradation of the superlattice was also followed by the powder X-ray diffraction technique (see Fig. 5). No considerable change was observed up to 500°C for the superlattice reflections as well as the lines from the ordinary cell. On the other hand, the superlattice reflections became diffuse or disappeared around 600°C. (The octatitanate structure itself was preserved up to the onset of the exotherm at 940°C, where it was disproportionated into $Rb_2Ti_6O_{13}$ and TiO_2 (*3*).)

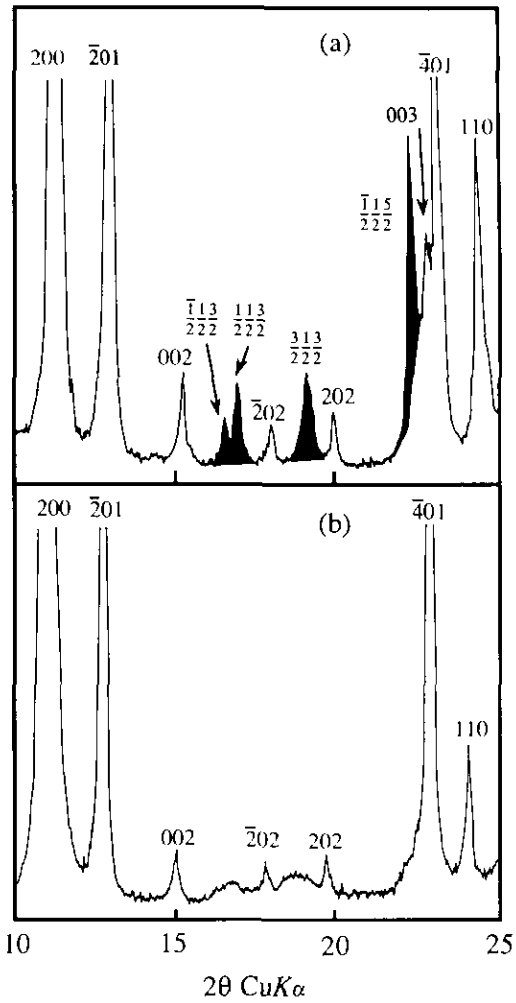

FIG. 5. X-ray powder diffraction patterns for the material heated (a) at 500°C and (b) 600°C. The filled reflections are attributable to the supercell.

Model of Rb Ion Ordering

The superlattice effect observed may be due to an ordered accommodation of Rb ions in the tunnel. Structural models for Rb ion ordering were constructed through the following procedures on the basis of the diffraction data obtained above.

(i) Rb ions are constrained in distorted cubic sites which are comparable to those in $K_2Ti_8O_{17}$. The close similarity in ionic size between K and Rb (*16*) gives a strong support for the similar coordination style. This was also suggested by the (010) high-resolution lattice image (*14*).

(ii) Six accommodation modes (A–F) in the unit tunnel are possible as shown in Fig. 6. Two of four pseudocubic sites, M_1, M_1', M_2 and M_2' in Fig. 1, are occupied by Rb ions.

(iii) Modes A & B, C & D, and E & F should be coupled along the b and c axes; for example, mode A should be followed by B in both of the directions, as shown schematically in Fig. 7. This is required because the reciprocal lattice sections of $h0l^*$ and $hk0^*$ did not exhibit superlattice reflections, which means that superposition of two of the modes in Fig. 6 along the b and c axes should average out the Rb ion distribution. This procedure results in three kinds of two-dimensional sheets of Rb ions and vacancies depending on the three pairs.

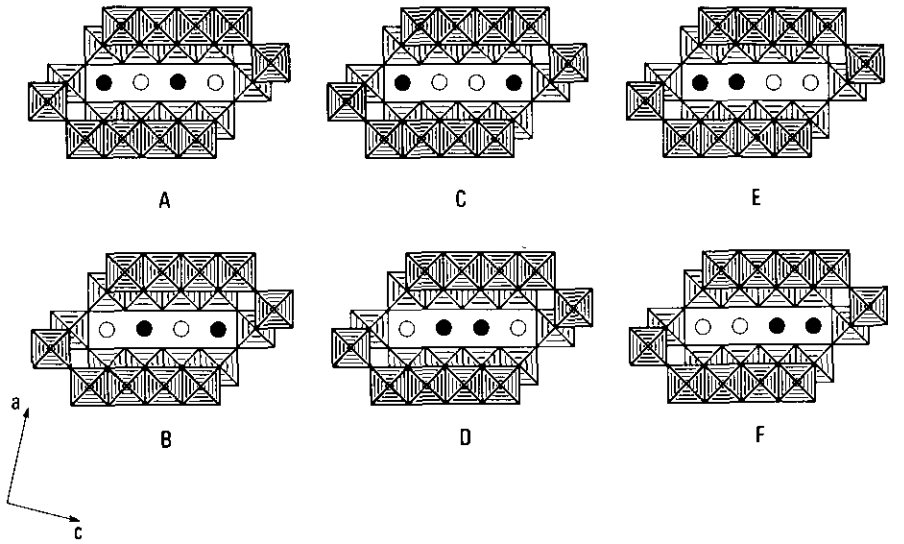

FIG. 6. Possible cation distributions in the unit tunnel. Filled circle, Rb ion; open circle, vacancy.

(iv) The last step in constructing models for the Rb ion ordering consists in making an array of the two-dimensional sheets along the *a* axis. Two types of stacking sequences are possible for each of the sheets composed of the paired models, such as A & B, C & D, or E & F. The example for the pair of A & B is –([A–A]–[B–B])– and –([A–B]–[B–A])– along the *a*. Hereafter, the square and round parentheses are used to express the limits of the sub- and super cell, respectively. Note that these two arrays produce the twinned superlattices of symmetry shown in Fig. 3.

The X-ray diffraction intensities for the superlattice reflections have been calculated in order to determine which pair is likely. The calculations involved Rb ions arranged in a fashion based on the pairs of A & B, C & D, and E & F. Their atomic coordinates were derived from the ideal drawings of the structural models. It was assumed that the individual twin components are contained in equal amounts. The observed intensities give a better matching toward the calculated values (corrected for Lorentz-polarization terms) for the model built up from the pair of A & B, rather than those from C & D and E & F, as follows:

Reflections	Observed	A & B	C & D	E & F
$\bar{\frac{1}{2}}, \frac{1}{2}, \frac{3}{2}$	24	16	100	100
$\frac{1}{2}, \frac{1}{2}, \frac{3}{2}$	36	44	91	57
$\frac{3}{2}, \frac{1}{2}, \frac{3}{2}$	40	67	54	20
$\bar{\frac{1}{2}}, \frac{1}{2}, \frac{5}{2}$	100	100	5	0.4
$\frac{7}{2}, \frac{1}{2}, \frac{3}{2}$	32	60	4	0.5

Furthermore, the models based on the pairs of C & D and E & F are unlikely because the accommodation modes D, E, and F are not favorable due to coulombic repulsion between cations directly contacted.

The schematic representation of the structural models derived at the conclusion of the above procedures is illustrated in Figs. 8a and 8b. The models (a) and (b) correspond to the reciprocal cells of (b) and (c)

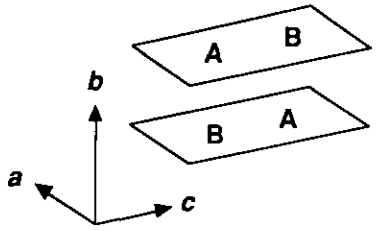

FIG. 7. Required sequence of the cation accommodation modes along the b and c axes.

in Fig. 3, respectively. It is to be emphasized that the models can be intergrown with each other, as visualized in Fig. 9. Two structures, which appear to be approximately equivalent in terms of lattice energy, may facilitate the introduction of thin domains which alternate along the a axis. This is consistent with the short range coherence revealed by the above-mentioned lateral distortion of the superlattice spots along the a^*.

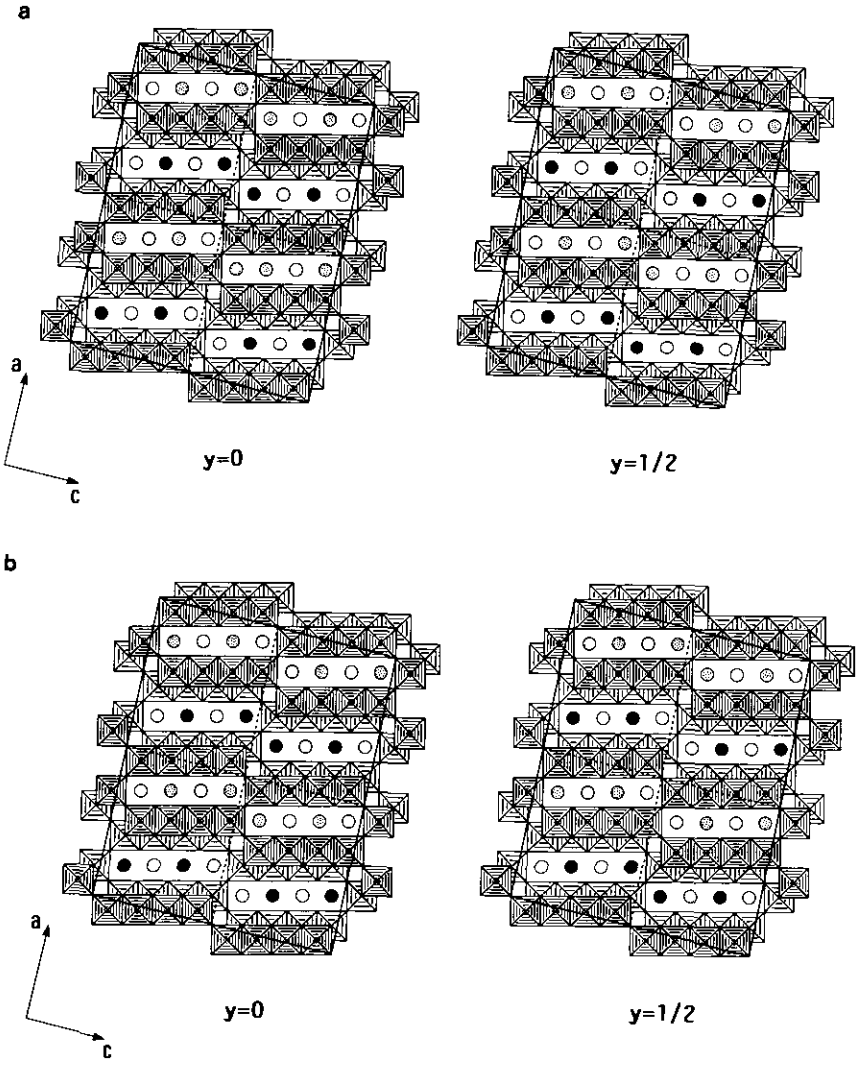

FIG. 8. Structural models for Rb ion ordering. Projection along the b axis. Filled circle, Rb ion on $y = 0$ and $\frac{1}{2}$ of the supercell. Stippled circle, Rb ion on $y = \frac{1}{4}$ and $\frac{3}{4}$. Open circle, vacancy. The super- and subcells are enclosed by full lines and broken ones, respectively.

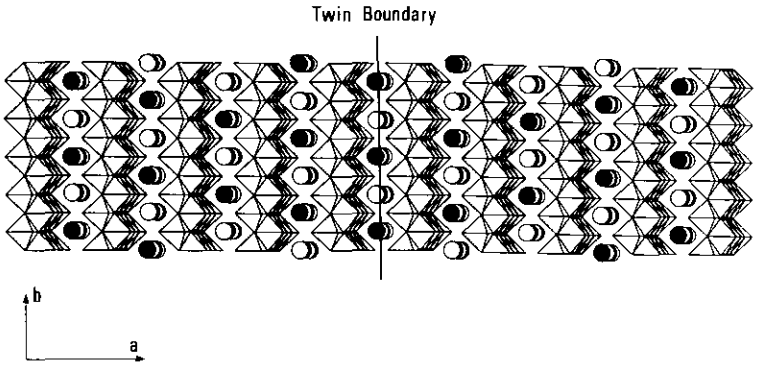

FIG. 9. Twin formation of Rb ion ordering. Projection along the c axis. Filled circle, Rb ion; open circle, vacancy. The solid line represents the twin boundary; the left hand side corresponds to the model shown in Fig. 8a and vice versa.

The models contain the chains of –([Rb]–[□])– and –([Rb–□–Rb–□]–[□–Rb–□–Rb])– (□: vacancy) along the b and c axes, respectively. The cations arrange in such a manner to avoid a direct contact except for the proximity between the cation at one end of a unit tunnel and the other ion at another end of the next tunnel along the c. This close contact may be tolerated due to a screening effect of the oxygen atom which bridges the titanate frameworks. The positive charge of the cations is shielded more effectively along the a axis by the host lattice of $[Ti_8O_{17}^{2-}]_\infty$. This gives a reasonable explanation for the observation that the cation correlation in this crystallographic direction was destroyed easily.

Extension of the Ordering Model to the Case in $K_2Ti_8O_{17}$

In this study, no superlattice was observed for $K_2Ti_8O_{17}$ although the electron diffraction measurement was limited to room temperature. The Rietveld refinement indicated that the K ions were statistically distributed; $\frac{2}{3}$ in M_1 site and remaining $\frac{1}{3}$ in M_2 (*14*). These facts suggest a K ion accommodation model in which the sequences, –[K]–[K]–[□]– and –[K]–[□]–[K]–, are randomly intergrown in the row of M_1 sites along the b, and the inverses, –[□]–[□]–[K]– and –[□]–[K]–[□]–, in the adjacent row of M_2. This arrangement does not give rise to any supercell periodicity along the b and c axes.

Patarin and Marchand, on the other hand, reported diffuse superlattice reflections in the electron diffraction pattern of $0kl^*$ zone for $K_2Ti_8O_{17}$ at an ambient temperature and below (*15*). The superlattice satellites they observed were incommensurate with respect to the b axis while commensurate along the c with multiplicity of 2. The incommensurability parallel to the b varied continuously from 0.365 at 77 K to 0.475 at room temperature.

The results of Patarin and Marchand may be interpreted by extending the structural models for $Rb_2Ti_8O_{17}$. The doubled dimension of the c axis may be caused by the alternating alignment of K ions and vacancies, evolving chains of –[K–□–K–□]–[□]–K–□–K]–. The incommensurate periodicity along the b axis and its temperature dependent nature may be accounted for by a random intergrowth of two kinds of chains; –[K]–[□]– and –[K]–[K]–[□]– (or –[K]–[□]–[K]) are intergrown, most likely in the row of M_1 sites, while the inverses, –[□]–[K]– and –[□]–[□]–[K] (or –[□]–[K]–[□]–), should be coupled in the M_2 row. If one couple of the three-membered components, –[K]–[K]–[□]– + –[□]–[□]–[K]– or –[K]–[□]–[K]– + [□]–[K]–[□]–, is pre-

dominant, the intermediate periodicity (0.33 – 0.5) can be produced by mingling the sequences at various ratios. For example, an incommensurability of 0.4 is elucidated by the 2-to-3 intergrowth where the chain of –{[K]–[□]}–{[K]–[K]–[□]}–{[K]–[K]–[□]}–{[K]–[□]}–[K]–[K]–[□]}– and its inverse, –{[□]–[K]}–{[□]–[□]–[K]}–{[□]–[□]–[K]}–{[□]–[K]}–{[□]–[□]–[K]}–, are situated in the M_1 and M_2 rows, respectively.

The reason for the difference between our results and those of Patarin and Marchand is unknown. Preparation temperatures and annealing processes may be responsible.

Comparison of the Cation Distribution in K- and Rb-Octatitanates

A larger number of K ions tends to be situated in M_1 site rather than in M_2 while Rb ions are perfectly ordered between these two sites. The cation distribution in octatitanates is dominated principally by two factors; site potential (one-atom model) and repulsion between the cations. The site potential for M_1 is expected to be deeper than that for M_2. Note that M_1 site has an 11-fold coordination environment (one oxygen atom is missing from the ideal cubic site) while M_2 gives a 10-fold coordination. In the case of K ions, the site potential term appears to compensate for the unfavorable proximity between a K ion and another above or below along the b, which traps a majority of the cations in M_1 site. The substitution of K with Rb does not make a considerable elongation in the b axis (0.011 Å) (*3*), even though the Rb ion (10–12-fold coordinated) surpasses the K ion in size by 0.07–0.08 Å (*16*). This implies that the direct Rb–Rb contact along the b would give a more severe strain. Thus, the Rb ions arrange themselves to make their intercation distance as long as possible, as in the configurations in Fig. 8.

References

1. R. Marchand, L. Brohan, and M. Tournoux, *Mater. Res. Bull.* **15,** 1129 (1980).
2. R. Marchand, L. Brohan, R. M'Bedi, and M. Tournoux, *Rev. Chim. Miner.* **21,** 476 (1984).
3. T. Sasaki and Y. Fujiki, *J. Solid State Chem.* **83,** 45 (1989).
4. S. Andersson and A. D. Wadsley, *Acta Crystallogr.* **14,** 1245 (1961).
5. A. Verbaere and M. Tournoux, *Bull. Soc. Chim. Fr.* 1237 (1973).
6. M. Dion, Y. Piffard, and M. Tournoux, *J. Inorg. Nucl. Chem.* **40,** 917 (1978).
7. I. E. Grey, I. C. Madsen, J. A. Watts, L. A. Bursill, and J. Kwiatkowska, *J. Solid State Chem.* **58,** 350 (1985).
8. J. Kwiatkowska, I. E. Grey, I. C. Madsen, and L. A. Bursill, *Acta Crystallogr. Sect. B* **43,** 258 (1987).
9. S. Andersson and A. D. Wadsley, *Acta Crystallogr.* **15,** 194 (1962).
10. A. D. Wadsley and W. G. Mumme, *Acta Crystallogr. Sect. B* **24,** 392 (1968).
11. M. Watanabe, Y. Bando, and M. Tsutsumi, *J. Solid State Chem.* **28,** 397 (1979).
12. L. Pauling, in "The Nature of the Chemical Bond", 3rd ed., p. 547, Cornell Univ. Press, Ithaca, NY (1960).
13. J. A. Watts, *J. Solid State Chem.* **1,** 319 (1970).
14. T. Sasaki, M. Watanabe, Y. Fujiki, Y. Kitami, and M. Yokoyama, *J. Solid State Chem.* **92,** 537 (1991).
15. J. Patarin and R. Marchand, *C. R. Seances Acad. Sci. Ser. II* **300,** 667 (1985).
16. R. D. Shannon, *Acta Crystallogr. Sect. A* **32,** 751 (1976).